Volt-ampere characteristics of a nitrogen DC plasma arc with anode melting*

Zhao Peng(赵 鹏)[a)b)†], Ni Guo-Hua(倪国华)[a)], Meng Yue-Dong(孟月东)[a)], and Nagatsu Masaaki(永津雅章)[b)]

[a)] *Institute of Plasma Physics, Chinese Academy of Sciences, Hefei* 230031, *China*

[b)] *Graduate School of Science and Technology, Shizuoka University,* 3-5-1, *Johoku, Nakaku, Hamamatsu,* 432-8561, *Japan*

(Received 20 September 2012; revised manuscript received 30 November 2012)

The characteristics of a nitrogen arc using a graphite cathode and a melting anode in a pilot-scale plasma furnace are investigated. The voltage is examined as a function of current and apparent plasma length. The voltage increases non-linearly with the increase of apparent plasma length, with the current fixed. The experimental data so obtained are compared with the predictions of the Bowman model for the electric arc, and with numerical simulations as well. The level of agreement between the experimental data at the melting anode and the numerical predictions confirms the suitability of the proposed the Bowman model. These characteristics are relevant to the engineering design and evaluation of a DC plasma furnace and reactor for the treatment of hazardous fly ash waste.

Keywords: volt-ampere, plasma length, melting anode plasma arc, fly ash

PACS: 47.65.–d, 47.75.+f, 52.25.Dg, 52.25.Fi **DOI:** 10.1088/1674-1056/22/6/064701

1. Introduction

The thermal plasma has many useful characteristics, such as a high current, a high temperature, and intense radiation power. Many previous studies have shown that the thermal plasma is a promising technology for the vitrification of hazardous fly ash from a solid waste incinerator (MSWI) in an urban area.[1–3] It achieves detoxification and volume-reduction. The higher temperatures and energy densities possible in plasma systems promote chemical reactions, allow shorter residence time, and make large throughputs possible in a pilot-scale furnace.

We focus on the DC nitrogen plasma arc, which is a kind of stabilized plasma arc that is easily controlled. The principal advantages that DC arc plasma offers to the treatment processes are[1,2]

(i) reduced flicker,

(ii) improved arc stability,

(iii) stronger bath stirring action,

(iv) higher power inputs to the bath,

(v) reduced electrode consumptions,

(vi) reduced noise emission over equivalent AC furnaces.[1]

The effects of introducing nitrogen through a hollow graphite cathode have been studied.[1–3] Numerical simulation and calculation of the plasma arc were rapidly developed in order to test and verify experimental data in most previous studies.[4–6] It is now generally accepted that this technique improves arc stability (i.e., reduces fluctuations and noise) by providing a homogeneous unreactive atmosphere for the arc, and by establishing a low-resistance conducting path. The gas flow also affects the spatial stability of the arc column to a certain degree and increases the transfer of energy to the melted slag, which is connected as the anode. The increased stability, reduced arc flare, improved power factor, increased heating rate, and reduced consumption of the refractories were reported, compared with those of similar systems using other solid electrodes.[7,8]

The arc volt-ampere characteristic (VAC) is an integral indicator of the general behavior of all the arc parts, among which the most important are the near-electrode layers and positive column. It is usually assumed that a rising character in VAC reflects a stabilized positive column, which indicates the presence of some factors that restrict the widening of the arc cross section with the increase of current, such as a cooled wall, gas vortex, or longitudinal magnetic field. In this case, the voltage dropping off along the stabilized part of arc discharge increases with current increasing, which causes the general arc voltage to rise. Both the anode and cathode near-electrode layers should have similar influences. Of these factors, the least clear is the reaction of the anode spot in response to changing current, because its mechanism is unknown.[9–11]

In the present paper, we investigate the influences of the melting anode and various parameters such as the current, the terminal voltage, and especially the plasma length, on the characteristics of the plasma arc. In this report we describe the experiments and numerical simulations that are carried out to determine the basic characteristics of the DC arc operating in the pilot-scale DC plasma melter developed at the Institute of Plasma Physics, Chinese Academy of Science (ASIPP). These

*Project supported by the National Natural Science Foundation of China (Grant No. 21171169) and the Knowledge Innovation Project of the Chinese Academy of Sciences (Grant No. O45CF3A211).

†Corresponding author. E-mail: pzhao@ipp.ac.cn

© 2013 Chinese Physical Society and IOP Publishing Ltd

characteristics are valuable as a VAC process monitor or control variables and will provide valuable information for the engineering design and evaluation of DC plasma furnace.

2. Pilot-scale DC arc systems utilizing graphite electrodes

Figure 1 shows the process flow chart of the experimental apparatus used in this paper for plasma vitrification. The system consisted of a plasma furnace, an electrical power supply, a slag gathering system, a metal gathering system, waste gas pollution abatement devices, and an automatic control system. Plasma gas was supplied through a hole along the axis of the graphite cathode, and high-temperature plasma was generated by the electric discharge as shown in Fig. 2. The energy of the plasma was transferred to the anode of the furnace to melt fly ash, which was fed into the vessel continuously. Both heat and ultraviolet radiation from the arc can decompose dioxins into small molecules. Once melted, the slag continuously escaped from the furnace, together with the hot waste gas as shown in Fig. 3. At the same time, the metals sank to the bottom of the furnace due to their specific gravity and were discharged from the furnace periodically. The waste gas entered into the pollution abatement devices to be scrubbed.[1] It was reported that 48.44% of the total energy input was supplied to the bath, and more than 59% of the total energy was transported by convection.[7,12]

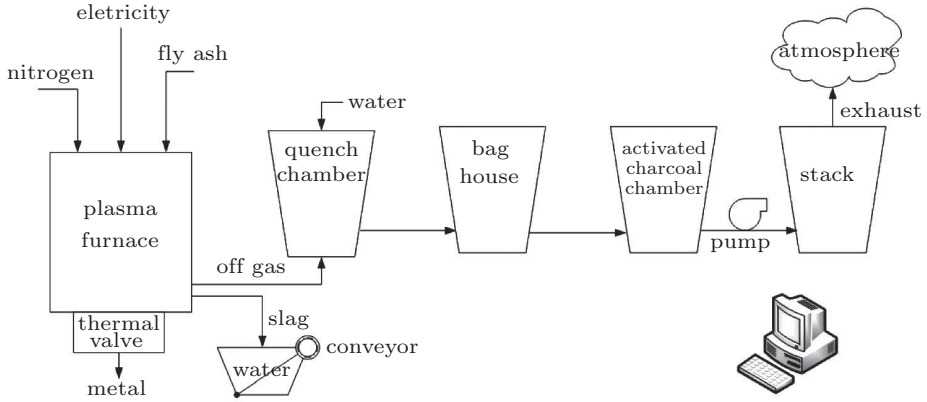


Fig. 1. Flow chart of the plasma vitrification process.

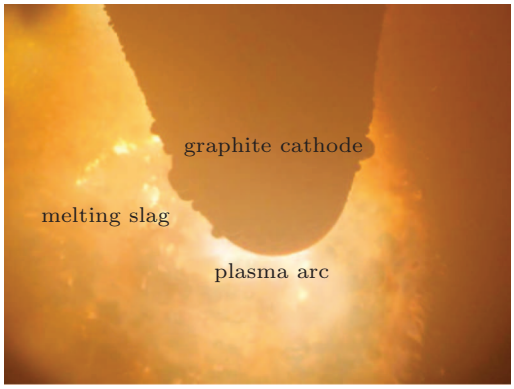


Fig. 2. (color online) Photo of DC arc and melting slag in experiment.

Major specifications of the experimental equipment that generated the plasma arc employed in this study are as follows: The maximum rating specifications of the electric power source are DC 160 V in voltage, 1500 A in current, and 240 V in open-circuit voltage.

The electrical power supply was a continuously adjustable stabilized power supply with a maximum DC output of up to 240 V/1500 A as shown in Fig. 4. The power supply enabled the arc current to be controlled in a wide range, and the thyristor-based system could adjust and set the maximum open-circuit voltage at four intermediate settings while still maintaining an output current up to 1500 A. This capability did match the power supply to the fly ash melting furnace.

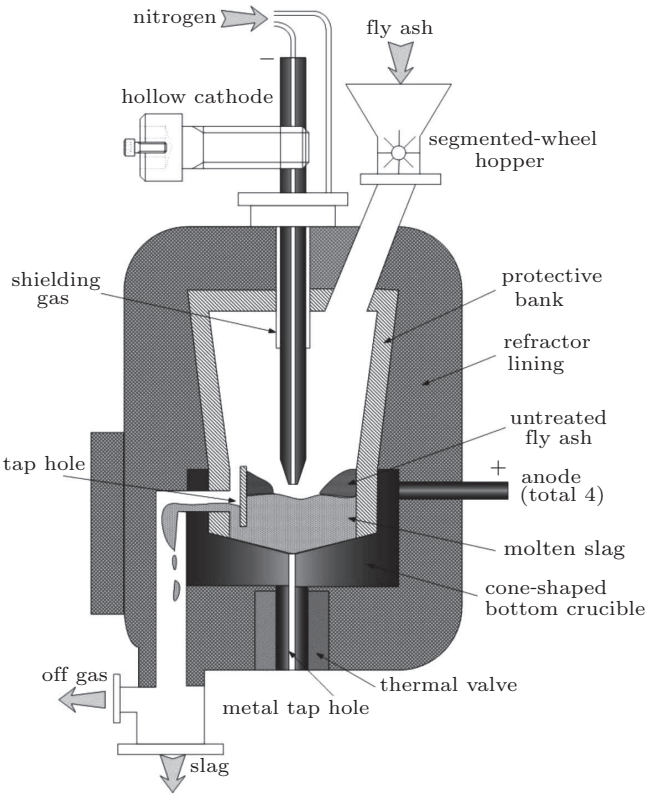


Fig. 3. Schematic diagram of vitrification furnace.

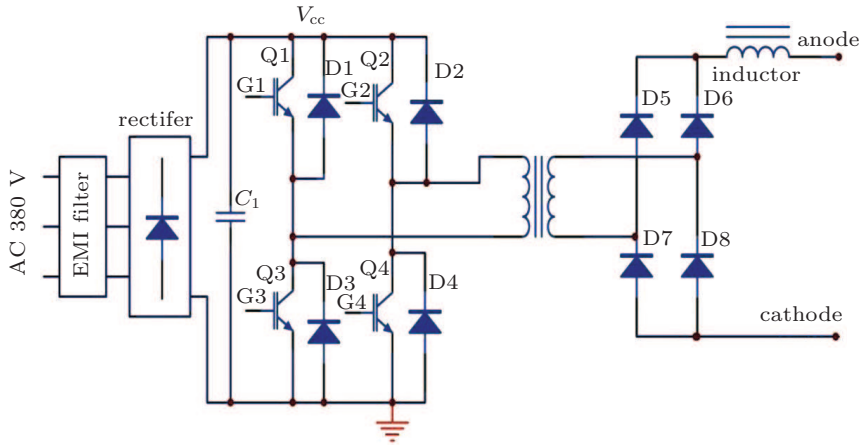


Fig. 4. (color online) DC power supply.

3. Experimental determination

3.1. Operation

Experimental conditions are shown in Table 1. The heating rates of fly ash were controlled to about 10 K/min. The molten slag was kept above 1700 K for 10 min. Operating procedures were used to maintain the operating temperature by controlling the DC plasma power.[2–5]

Table 1. Specifications of pilot plant.

Item	Specification
Melting furnace type	graphite-electrode plasma melting furnace
Plasma gas	nitrogen
Plasma gas velocity	2 m/s
Electric power	100 kW (100 V×1000 A)
Fly ash throughput	100 kg/h (0.0278 kg/s) rated capacity

Pure nitrogen was employed as both the plasma gas and the shielding gas. The chamber was evacuated and back-filled with nitrogen to a pressure of −100 Pa (gauge pressure).[1] Plasma gas flow rate was fixed at 140 scfh (12 L/min), and the comparison and simulation showed that this value increased stability and improved the heating rate.

3.2. Measurement

After 10-day steady operating, on the pilot plant furnace, tests were carried out to investigate the variations of arc voltage with arc length at various constant levels of arc current in a current range of 100 A∼700 A, and with the electrode at various known heights above the surface of the melted slag. The test may be performed with feed off, and shows the behavior of the voltage drop in the electric arc as a function of its length. A voltmeter was used to measure the voltage between the cathode and anode in the system. The length of the DC free arc established was measured from a scale attached to the vertical cathode drive system. Typical accuracy for measurement of the electrode position is on the order of 1 mm∼2 mm, so the source of error is negligible.[6]

Throughout the tests the electrode attachments, or arc roots, moved over the surface of the anode/melted slag, and around the periphery of the hollow cathode irregularly. The bore of the hollow 100-mm diameter graphite cathodes used was 10 mm. The arc root motion was probably related to the electron emission characteristics of the cathode surface, arc gas convection, seething slag, and electromagnetic effects, accompanied with erosion of the tip of the cathodes. It was observed that arc stability tended to increase with arc current increasing, and decrease with arc length increasing. When the higher open-circuit voltages up to 150-V DC was used in the plasma melting furnace, longer arcs could be maintained at the higher current.[8,13]

The free-arc voltage/current characteristics at constant arc length were determined from the experimental results and are shown in Fig. 5 (for currents greater than 700 A, the frequently changing flaring arc length endangered the power supply in our pilot-scale melter).

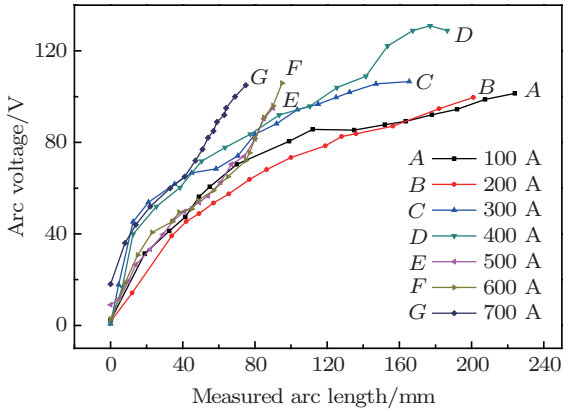


Fig. 5. (color online) Variations of arc voltage (V) with current and electrode separation/arc length (L) for DC free arcs.

4. Numerical simulation

4.1. Bowman model

The steady-state electrical behavior of the DC arc has been well described previously (Bowman *et al*., 1969; Bowman, 1994),[14,15] effectively summarizing a large quantity of data from DC electrical arcs in a range of 1 kA∼10 kA. This work provides a description of how the arc voltage varies with arc length and current. The model uses the measured and extrapolated arc shapes to fit the calculated plasma conductivities and estimated temperature profiles. The high-intensity plasma arc has been modeled by Bowman to emanate from a relatively small attachment area on the graphite cathode, and extends down to the surface of the molten bath.

The assumptions include an axisymmetric arc and no interaction effects on the anode. The equation, which stems from a large quantity of data in a 1 kA∼10 kA range, is described as follows. Under the assumption of a parabolic distribution of electrical conductivity along the arc radius, the arc shape function allows the arc voltage to be obtained by integration. Several empirical Bowman's constants, together with a single variable parameter and the average arc resistivity, appear in the arc voltage expression. Variation of the arc resistivity then allows the model to fit the pilot or industrial plant data.

The final result of this model is an expression relating the voltage of the arc to its length and current. This is shown in Eq. (1), which shows arc voltage as a function of arc length for a range of different currents at a given nitrogen plasma resistivity of $\rho_a = 0.233\ \Omega{\cdot}\mathrm{m}$.[16]

$$V_a = \frac{I\rho_a}{m\pi}\left[-\frac{1}{a^2+ab}+\frac{1}{a^2+ab.\exp(mL_a)} + \frac{\ln(a+b)}{a^2}+\frac{mL_a}{a^2}-\frac{\ln[a+b.\exp(mL_a)]}{a^2}\right], \quad (1)$$

where

$$a = 3.2r_k, \quad (1a)$$

$$b = -2.2r_k, \quad (1b)$$

$$m = \frac{-1}{5r_k}, \quad (1c)$$

$$r_k = \sqrt{\frac{I}{\pi j_k}}. \quad (1d)$$

In Eq. (1), V_a is the arc voltage (V), I the current (A), L_a the arc length (mm); ρ_a the average arc resistivity through the conducting section of the arc column ($\Omega \cdot \mathrm{m}$); r_k the radius of the arc at the cathode surface (mm), which is determined by the value of the cathode-spot current density j_k, here $j_k = 3.5 \times 10^7$ A/m^2, which is estimated by Bowman equation (1), was used to produce expected values of arc voltage as a function of arc length and current for our furnace. The curves are shown in Fig. 6. The value used for the arc resistivity was that which gave theoretical curves that most closely resemble the experimental data.

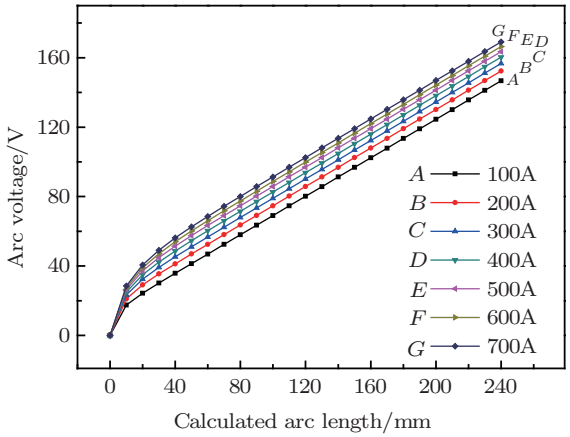


Fig. 6. (color online) Variations of arc voltage with current and arc length according to the Bowman model, for a given arc resistivity of $\rho_a = 0.233\ \Omega{\cdot}\mathrm{m}$.

The level of agreement achieved between the experimental data (as shown in Fig. 5) and the numerical prediction confirms the suitability of the Bowman model for describing the conditions in our furnace.

4.2. Numerical study of a free-burning nitrogen arc with melted fly ash anode

The cathode, arc plasma, and melting fly ash anode are described using a frame of cylindrical coordinates with axial symmetry around the arc axis. As shown in Fig. 7, the calculation domain was a cylinder of length 450 mm and radius 200 mm. The cathode had a cylindrical shape with a conical tip facing the plasma. The cathode length was 210 mm and its radius was 50 mm. The conical tip of the cathode had an included angle of 30 degrees and a flat tip of radius 10 mm. The anode was a melting slag of radius 200 mm, separated from the cathode by inter-electrode gaps of 80, 120, 160, 200, and 240 mm respectively.

4.2.1. Assumptions

i) The flow is assumed to be laminar, the electron and heavy particle temperatures are assumed to be equal (local thermodynamic equilibrium), and the effects of the non-collisional space-charge zone in front of both electrodes are neglected.

ii) An optically thin assumption is used, whereby light absorption is neglected. This assumption corresponds to a plasma temperature lower than 2×10^4 K.

iii) The current density at the cathode is assumed to be

constant and with an average value of 3.5×10^7 A/m^2 based on experimental information;

iv) The physical properties of the material, such as electrical conductivity, thermal conductivity, density, specific heat, enthalpy, and viscosity depend only on temperature.

v) The anode surface is considered to be flat, unperturbed by the arc pressure.[8,10]

vi) Chemical reactions in the molten pool are neglected.

vii) No vapor from the cathode or anode material is present.

4.2.2. Governing equations

The general mathematical formulation of this model can be found elsewhere.[6–12] Here, only a brief summary of the mathematical formulation is presented together with the discussion of some improvements on the model given by other authors. The governing equations and numerical method were extended from the model of Tanaka[17] and Sansonnens *et al.*,[18] to include convective effects of the molten fly ash anode. The mass continuity equation is

$$\frac{1}{r}\frac{\partial}{\partial r}(r\rho v_r)+\frac{\partial}{\partial z}(\rho v_z)=0, \tag{2}$$

where ρ, v_z, and v_r are the density, the axial, and radial velocities, respectively.

The radial momentum conservation equation is

$$\begin{aligned}&\frac{1}{r}\frac{\partial}{\partial r}(\rho r v_r^2)+\frac{\partial}{\partial z}(\rho v_r v_z)\\ &=-\frac{\partial P}{\partial r}+\frac{1}{r}\frac{\partial}{\partial r}\left(2r\mu\frac{\partial v_r}{\partial r}\right)\\ &\quad+\frac{\partial}{\partial z}\left(\mu\frac{\partial v_r}{\partial z}+\mu\frac{\partial v_z}{\partial r}\right)-2\mu\frac{v_r}{r^2}-j_z B_\theta.\end{aligned} \tag{3}$$

The axial momentum conservation equation is

$$\begin{aligned}&\frac{1}{r}\frac{\partial}{\partial r}(\rho r v_r v_z)+\frac{\partial}{\partial z}(\rho v_z^2)\\ &=-\frac{\partial P}{\partial z}+\frac{\partial}{\partial z}\left(2\mu\frac{\partial v_z}{\partial z}\right)\\ &\quad+\frac{1}{r}\frac{\partial}{\partial r}\left(r\mu\frac{\partial v_r}{\partial z}+r\mu\frac{\partial v_z}{\partial r}\right)+\rho g+j_r B_\theta,\end{aligned} \tag{4}$$

where P, μ, j_r, j_z, g, and B_θ are the pressure, the viscosity, the radial, the axial current density, the acceleration due to gravity, and the self-magnetic field, respectively.

The Maxwell equation is

$$B_\theta=\frac{\mu_0}{r}\int_0^r j_x\xi\,\mathrm{d}\xi. \tag{5a}$$

Since $j_z\gg j_r$, the self-induced magnetic field B_θ may be written as

$$\frac{1}{r}\frac{\partial}{\partial r}(rB_\theta)=\mu_0 j_z. \tag{5b}$$

Since

$$B_\theta=\frac{\partial A_r}{\partial z}-\frac{\partial A_z}{\partial r},$$

the above equation may be written as

$$\frac{\partial^2 A_z}{\partial z^2}+\frac{1}{r}\frac{\partial}{\partial r}\left(r\frac{\partial A_z}{\partial r}\right)+\mu_0 j_z=0, \tag{5c}$$

$$\frac{\partial^2 A_r}{\partial z^2}+\frac{1}{r}\frac{\partial}{\partial r}\left(r\frac{\partial A_r}{\partial r}\right)-\frac{A_r}{r^2}+\mu_0 j_r=0, \tag{5d}$$

where μ_0 is the permeability of vacuum, A_z and A_r are the axial and radial magnetic vector potential.

Current continuity requires that

$$\frac{\partial j_z}{\partial z}+\frac{1}{r}\frac{\partial}{\partial r}(rj_r)=0. \tag{6a}$$

Since

$$j=\sigma(-\nabla\phi),$$

the above equation may be written as

$$\frac{\partial}{\partial z}\left(\sigma\frac{\partial\phi}{\partial z}\right)+\frac{1}{r}\left(\sigma r\frac{\partial\phi}{\partial r}\right)=0, \tag{6b}$$

where σ is the electrical conductivity and ϕ is the electrical potential.

The energy equation is

$$\begin{aligned}&\frac{\partial(\rho C_p v_z T)}{\partial z}+\frac{\partial(\rho C_p r v_r T)}{r\partial r}\\ &=\frac{\partial}{\partial z}\left(k\frac{\partial T}{\partial z}\right)+\frac{1}{r}\frac{\partial}{\partial r}\left(kr\frac{\partial T}{\partial r}\right)-S_{\mathrm{R}}\\ &\quad+\frac{j_z^2+j_r^2}{\sigma}+\frac{5}{2}\frac{k_{\mathrm{B}}}{e}\left(j_z\frac{\partial T}{\partial z}+j_r\frac{\partial T}{\partial r}\right),\end{aligned} \tag{7}$$

where k is the thermal conductivity, C_p the specific heat, and S_{R} the radiation emission coefficient.

The governing equations of the anode (melting fly ash) region is normal computational fluid dynamics CFD model, which is not the emphasis and whose description requires several pages, so we just give the plasma governing equation.

4.2.3. Physical properties, boundary conditions, and numerical method

The shielding gas and working gas of the free-burning arc are assumed to be pure nitrogen. The shielding gas is introduced at a constant flow rate of 12 L/min from the outside of the cathode at the upper boundary. The working gas at a flow rate of 6 L/min is additionally introduced through the hole of the hollow cathode. Specifications and working conditions of the pilot plant are shown in Table 1. The required input parameters are the physical properties of nitrogen plasma,[16] graphite cathode, and melting fly ash[17] as shown in Table 2.

Table 2. Major physical properties of cathode, arc plasma, and anode.[16,17]

No.	Item	Physical properties	
1	cathode	thermal conductivity	139 W/m·K∼163 W/m·K
	(graphite)	electrical conductivity	10^5 A/V·m∼1.6×10^5 A/V·m
		specific heat	709 J/kg·K
		density	1600 kg/m^3
2	arc plasma	ionization potential	15.6 eV
	(nitrogen)	thermal conductivity	0.026 W/m·K∼6.347 W/m·K
		electrical conductivity	0∼13391 A/V·m
		specific heat	10^4 J/kg·K∼2.3×10^4 J/kg·K
		density	0.0013 kg/m^3∼0.8439 kg/m^3
		viscosity	1.756×10^{-5} kg/m·s∼2.427×10^{-4} kg/m·s
3	anode	melting point	1523 K
	(melted fly ash)	thermal conductivity	0.14 W/m·K∼2.8 W/m·K
		electrical conductivity	737312 A/V·m∼813579 A/V·m
		specific heat	1008 J/kg·K
		density	2800 kg/m^3
		viscosity	0.0003 kg/m·s∼2.77 kg/m·s

Table 3. Boundary conditions.

Boundary	T/K	ϕ/V	v_z/m·s^{-1}	v_r/m·s^{-1}	A_z	A_r
A–B (gas inflow)	500	$\partial\phi/\partial z=0$	inflow	0	$\partial A_z/\partial z=0$	$\partial A_r/\partial z=0$
B–C–D (cathode top)	3500	–	0	0	$\partial A_z/\partial z=0$	$\partial A_r/\partial z=0$
D–E (cathode wall)	1000	$\partial\phi/\partial z=0$	0	0	$\partial A_z/\partial r=0$	$\partial A_r/\partial r=0$
E–F (gas inflow)	500	$\partial\phi/\partial z=0$	inflow	0	$\partial A_z/\partial z=0$	$\partial A_r/\partial z=0$
F–G–H (wall)	1600	$\partial\phi/\partial z=0$	0	0	$\partial A_z/\partial z=0$	$\partial A_r/\partial z=0$
H–I (outflow)	1800	$(1/r)(\partial r\phi/\partial r)=0$	0	$(1/r)(\partial r\rho v_r/\partial r)=0$	$\partial A_z/\partial r=0$	$\partial A_r/\partial r=0$
I–J (anode surface)	coupled	coupled	0	0	coupled	coupled
I–L (wall)	1700	$(1/r)(\partial r\phi/\partial r)=0$	0	0	$\partial A_z/\partial z=0$	$\partial A_r/\partial z=0$
L–K (anode bottom)	1700	0	0	0	$\partial A_z/\partial z=0$	$\partial A_r/\partial z=0$
K–J–A (axis)	$\partial T/\partial r=0$	$\partial\phi/\partial z=0$	$\partial v_z/\partial r=0$	0	$\partial A_z/\partial r=0$	$\partial A_r/\partial r=0$

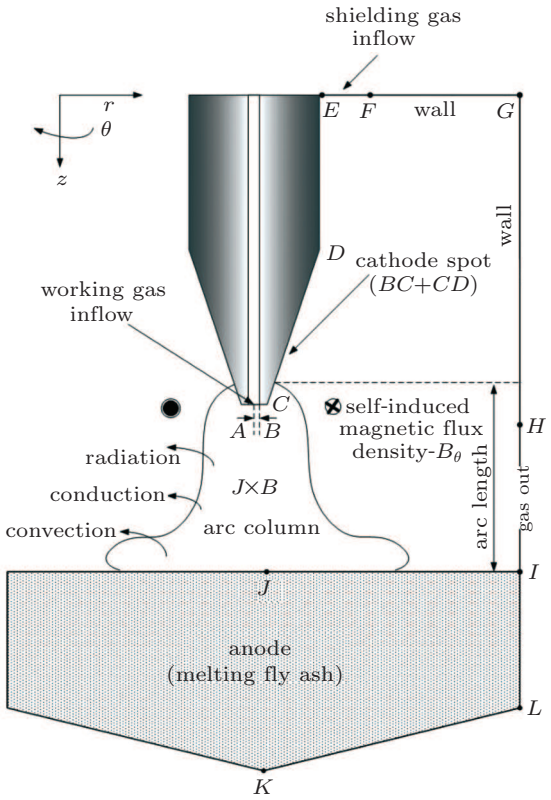


Fig. 7. Schematic illustration of the simulation domain.

The boundary conditions are presented in Table 3. The calculation domain includes the plasma region and the anode (melting fly ash) region, according to the actual requirements of the calculation. Although the solid cathode region is not included in the calculation domain, its boundary conditions are considered during simulation as shown in Table 3. In particular, the anode surface *I–J* is set as the couple boundary condition in the user defined function (UDF) of FLUENT, which means that the data of the plasma region and anode region could be exchanged through the couple boundary condition until convergence.

We assume that the differential equations (2)–(7) are solved iteratively by the SIMPLEC numerical procedure for the whole region of arc melting process as shown in Fig. 7. All governing equations, subject to their corresponding boundary conditions, are cast and solved simultaneously using the commercial CFD code FLUENT.

The output can include two-dimensional distributions of temperature, velocity, electric potential, current density, pressure, and magnetic field. Here only the distribution of electric potential is discussed, and the other arc characteristics are investigated beyond the scope of this paper. Figures 8 and 9 show the distributions of electric potential for the inter-electrode gaps of 80, 120, 160, 200, and 240 mm, and currents of 100 A and 700 A respectively.

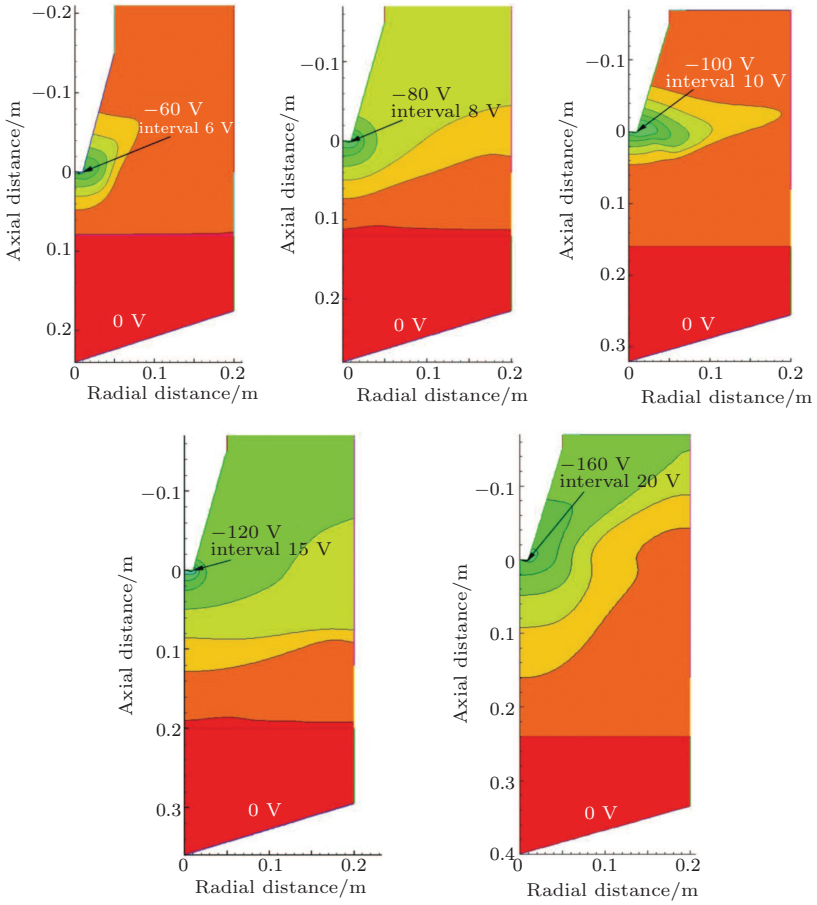


Fig. 8. (color online) Distributions of electric potential (V) for inter-electrode gaps of 80, 120, 160, 200, 240 mm respectively, and current of 100 A.

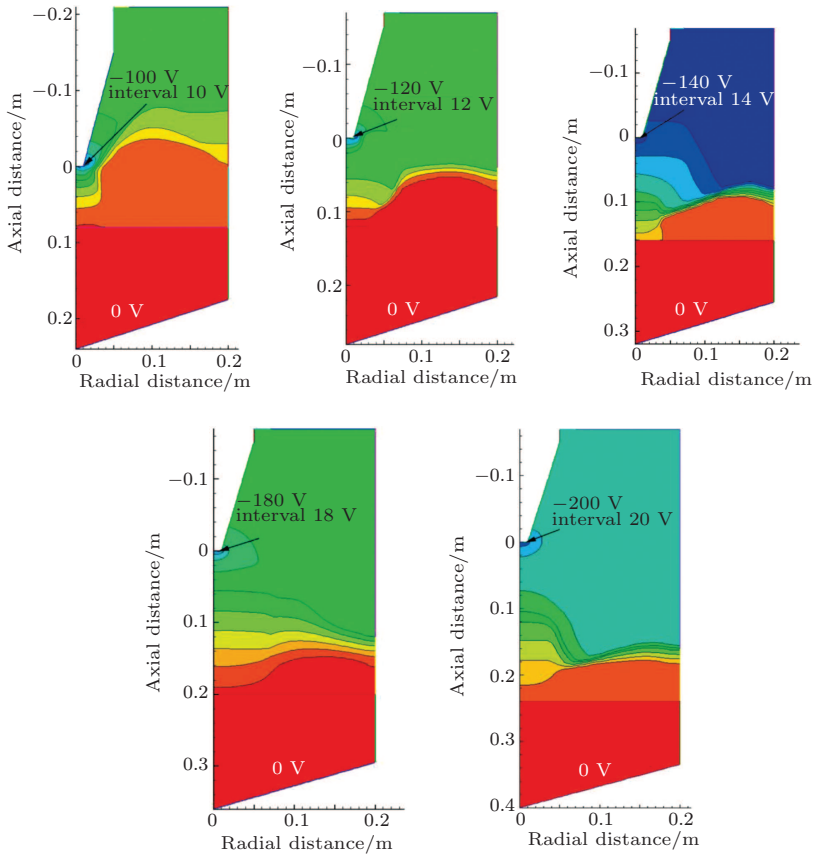


Fig. 9. (color online) Distributions of electric potential (V) for inter-electrode gaps of 80, 120, 160, 200, 240 mm respectively, and current of 700 A.

5. Discussion

In Figs. 5 and 6, the differences between the measured and the computed arc voltage values are rather constant, in considering the measurement uncertainty (±10 V) in the 100 A∼200 A current range. In experiments, the flow of plasma gas through the hollow cathodes stabilizes the arcs and imparts a degree of stiffness to the arc columns. But the anode is melting slag, which is boiling, unstable, and causes arc drifting and flaring. The arc is therefore extremely mobile, with rapid oscillations around its axis and the consequent voltage fluctuations that affect the measurements. We estimate that the error of experimental measurement should be within ±10%. But after many repeated experiments, the trend indicates the effective electrical characteristics of the arc in the furnace.

Increasing the distance between the electrodes leads to higher voltages due to the increased resistance of the arc. In particular, Bowman model predicts an increase in arc voltage, owing to higher current flow and a larger electrode gap. From Fig. 6, the voltage increases by about 6 V∼12 V for every 10 mm increase in the arc length. This value is in agreement with the experimental results in Fig. 5. The longer (240-mm length) arc also shows a rising voltage–current characteristic that is a typical of high intensity arcs. It is generally observed in Fig. 6 that the effect of a given parameter on voltage seems to be rather independent of the other values, i.e., no particular interaction appears between the factors.

From Fig. 6, the arc voltage/length characteristics of arcs exhibit a linear relationship between the arc voltage and arc length, which is more obvious at a long arc length. The behavior of a very short, root-dominated arc is nonlinear, owing to the absence of any fully developed arc column or equilibrium plasma region, the effects of electrons, ions, etc.[8] In theory, the characteristics are almost identical, irrespective of the current (Fig. 5) at currents up to around 700-A DC and arc lengths, or electrode separations, up to approximately 220 mm. But the arc voltage increases the plasma length because the convection heat loss increases in proportion to the apparent plasma length, and the pinch effect causes self-constriction of the arc, thereby increasing its resistance, especially at increasing currents, the elongation of the arc column due to the influence of electromagnetic and convective forces, and rotational movement of the attachment points over the surfaces of the electrodes. Especially, for the arc during melting, the flue gas flow will make the arc column unstable and moving, which is inevitable during melting fly ash. Previous research indicated that the arc column voltage gradient was lowest, generally, at a given value of current, when arcing was onto a melting anode.[8]

The slopes of the arc voltage/length characteristics represent the mean electric field strength, or voltage gradient, within the arc columns. As shown in Table 4, the slope values in Fig. 5 vary from 0.45 V·mm^{-1} to 3.14 V·mm^{-1}. The range of values is in close agreement with the 0.61 V·mm^{-1} to 2.85 V mm^{-1} reported in the result of Bowman model as shown in Fig. 6. Higher arc column voltage gradients are observed with molten fly ash anodes at 700 A. This anomalous behavior may be due to the more pronounced wander of the anode root over the surface of a melting anode and the influence of the crucible walls, since this result corresponds to the highest current used in the 100-kg furnace.[3]

Table 4. Slopes of the arc voltage/length characteristics of Figs. 5 and 6.

Line	Current/A	Slope/V·mm^{-1} in Fig. 5	Slope/V·mm^{-1} in Fig. 6
A	100	0.64 to 2.56	0.61 to 1.75
B	200	0.69 to 2.03	0.63 to 2.10
C	300	0.49 to 1.18	0.65 to 2.33
D	400	0.45 to 1.65	0.67 to 2.50
E	500	0.96 to 2.31	0.68 to 2.64
F	600	0.99 to 2.35	0.69 to 2.75
G	700	1.4 to 3.14	0.70 to 2.85

Table 5. Arc voltage (V) together with current and electrode separation/arc length (L) of Figs. 8 and 9.

Current/A	Arc voltage (V) with electrode separation/arc length (mm)				
	80 mm	120 mm	160 mm	200 mm	240 mm
100	60	80	100	120	160
700	100	120	140	180	200

Voltage, or known as electrical potential difference or electric tension is the difference in electric potential between two points, or the difference in electric potential energy per unit charge between two points. Figures 8 and 9 show the distributions of electric potential for inter-electrode gaps of 80, 120, 160, 200, and 240 mm, and currents of 100 A and 700 A respectively. From the distributions of electric potential, we can calculate the voltage between the cathode and anode, as shown in Table 5. By comparing Table 5 with Fig. 5, the voltages of numerical simulation are slightly higher than the experimental data, but the distribution trends of the voltages are almost the same. The difference between simulated and experimental data may be due to the fact that the measuring points of electric potential are at the outer ends of electrodes, not the discharging ends. So the voltages of experimental measurement include electrode voltage drop and electrode sheath drop.

Thus, the assumption that arc length is equal to the electrode separation is valid in the case of the DC free arc. The voltage/current characteristics for the free DC arc changes from negative to positive dynamic resistance at currents above approximately 250 A such that the increasing of current leads to an increased arc voltage. A contributing factor to this may increase in voltage due to the increase in arc length caused by

movement and spatial distortion of the arc column at higher currents under the influence of gas dynamic and electromagnetic forces.

6. Conclusions

The role of pilot-scale DC arc plasma systems in the research and development of a waste treating process is clear and vital. In this paper, we present the results of an experimental and numerical study on free DC arc characteristics in nitrogen.

The main conclusions are as follows.

(I) The voltage is examined as a function of current and apparent plasma length. The voltage increases non-linearly with the increase of the apparent plasma length with current fixed.

(II) The voltage gradient, V/L, remains almost constant irrespective of the apparent plasma length in the Bowman model results for $L > 50$ mm. However, the voltage gradient is higher for the experimental results. This anomalous behavior may be due to the more pronounced wander of the anode root over the surface of a melting anode and the influence of the crucible walls.

(III) The voltage/current characteristics for the free DC arc changes from negative to positive dynamic resistance at currents above approximately 250 A such that the increasing of the current leads to an increased arc voltage.

(IV) From the simulated distributions of electric potential, we can calculate the voltage between the cathode and anode. The simulated voltages are higher than the experimental data. This result may be due to the fact that the measuring points of electric potential are at the outer ends of electrodes, not the discharging ends.

The results of this study on the characteristics of electric arcs operating in the pilot-scale DC plasma arc systems provide an empirical and theoretical basis for the design and development of larger systems in which the evaluation of plasma heating processes can be continued. A demo-scale plasma furnace of up to 1-MW power has been planned and designed in ASIPP.

References

[1] Zhao P, Ni G H, Jiang Y M and Chen L W 2010 *J. Hazard. Mater.* **181** 580
[2] Kim H I and Park D W 2004 *J. Ind. Eng. Chem.* **10** 234
[3] Heberlein J and Murphy A B 2008 *J. Phys. D: Appl. Phys.* **41** 1
[4] Li H P and Chen X 2002 *Chin. Phys.* **11** 44
[5] Lan C H, Lan C Z, Hu X W, Chen Z Q and Liu M H 2009 *Chin. Phys. B* **18** 2412
[6] Liu X H, He W, Yang F, Wang H Y, Liao R J and Xiao H G 2012 *Chin. Phys. B* **21** 075201
[7] Zhao P, Meng Y D, Yu X Y and Chen L W 2009 *Plasma Sci. Technol.* **11** 206
[8] Knight R, Murawa M J, Girgis N M and Reid K J 1990 *Plasma Chem. Plasma Process.* **10** 359
[9] Zhang W, Roy G G, Elmer J W and DebRoy T 2003 *J. Appl. Phys.* **93** 3022
[10] Lee H J, Plaksin V Y and Riaby V A 2007 *Thin Solid Films* **515** 5197
[11] Reynolds Q G and Jones R T 2004 *J. S. Afr I. Min. Metall.* **4** 1
[12] Nanzyou T 1998 *Arc Phenomena of DC Arc Furnace* (Beijing: Metallurgical Industry Press) p. 120
[13] Bini R, Monno M and Boulos M I 2007 *Plasma Chem. Plasma Process.* **27** 359
[14] Jones R T, Reynolds Q G and Alport M J 2006 *Miner. Eng.* **15** 985
[15] Jordan G R, Bowman B and Wakelam D 1970 *J. Phys. D: Appl. Phys.* **3** 1089
[16] Boulos M I, Fauchais P and Pfender E 1994 *Thermal Plasmas: Fundamentals and Applications* (New York: Plenum Press) p. 403
[17] Tanaka M, Terasaki H, Ushio M and Lowke J J 2003 *Plasma Chem. Plasma Process.* **23** 585
[18] Sansonnens L, Haidar J and Lowke J J 2000 *J. Phys. D: Appl. Phys.* **33** 148